Int. J. Heat Mass Transfer. Vol. 35, No. 5, pp. 1103–1114, 1992
Printed in Great Britain

0017–9310/92 $5.00 + 0.00
Pergamon Press Ltd

The drying-induced deformations of a clay plate

J.-M. COLLARD, G. ARNAUD and J.-P. FOHR
LESTE (LET/URA 1403), 40, Avenue du Recteur Pineau, 86022 Poitiers, France

and

A. DRAGON
L.M.P.M. (URA CNRS 863) ENSMA, rue Guillaume le Troubadour, 86000 Poitiers, France

(*Received* 12 *June* 1990 *and in final form* 28 *May* 1991)

Abstract—This paper aims to study the drying-induced deformations of a clay plate exposed on one side to an air drying. The drying model is a diffusive one with material coefficients adjusted on drying kinetics. The stress–strain relationship is elastic/viscoplastic with a Mohr–Coulomb yield criterion. The corresponding six material coefficients are determined from specific experiments: shrinkage, triaxial compression of cylindrical specimens under monotone loading and creep. Some coefficients are moisture dependent and hence introduce a link between the mass transfer and mechanical fields. The results of the calculations performed are in agreement with experimental results for the plate deformation.

1. INTRODUCTION

THE PRODUCTS of baked earth are useful in building. In order to increase productivity, the tile and brick industry want to improve the production quality and thus reduce the deformation of the pieces, which can occur during the manufacturing.

During drying, the exhaust of the moulding water introduces a shrinkage which modifies the size of the pieces. If the drying is not homogeneous in the bulk, deformations appear and beyond a certain limit lead to a rejection of a piece. It is especially the case in tiles which cannot correctly adjust themselves when too large deformation is perceptible.

Thus, the improvement of drying processes needs a model of strain induced by a heterogeneous drying, the latter determined itself with the mean of mass transfer appropriate model. This double problem is complex and concerns two different scientific areas: heat and mass transfer and deformation. Considering drying and deformation together is always a difficult task which requires a compromise on the refinement of each partial modelling. The description of particular aspects, the nature of the material and the geometry must be a guidance for this compromise. The drying models were perfected in recent years, and can express most of the physical properties of the porous material as capillarity, vapour diffusion, liquid and gas flows [1, 2]. These models involve the knowledge of many parameters, determined from specific experiments. When the deformation can be confined in an elastic domain, the association is easier and it is possible to refine the drying model [3].

The deformation models, deriving from soil mechanics, express combined properties of elasticity, plasticity and viscosity of the material [4]. As the solution procedure, for example using a finite element method, the parameters are frequently taken to be independent of the water content [5].

The drying behaviour of the clay employed in our analysis is very regular, as shown in the drying kinetics diagrams; we thus choose a two-parameter diffusive model sufficient to express the properties of drying. As the deformation model should evaluate permanent strains after drying, an elastic/viscoplastic one is adequate with the corresponding parameters depending on water content. The deformation model is directly influenced by the drying model through the shrinkage, but the drying model considered is independent of the deformation.

The material studied is a particular kind of clay with a small percentage of sand used in a tile factory. The rheologic properties can differ from one site to another because clay is subject to a great range of species. Thus the obtained coefficients are particular and cannot be applied directly to another clay. The shapes of tiles are diversified and frequently complex to describe. We have chosen a simple plate shape and assume the possibility of large deformations where a single face is subjected to air drying.

2. THE DRYING STUDY OF CLAY PLATE

The physical properties of clay paste are given in Table 1. As the drying is heavily dependent on the

Table 1. Physical properties of clay paste

Distribution of grain size (Fig. 16)
Plastic limit 26.7%; liquid limit 56.7%
Specific surface 119 $m^2 g^{-1}$

NOMENCLATURE

C	cohesion parameter
D	diffusion coefficient
e	thickness of the clay plate (or half thickness for a plate submitted to a symmetrical drying air)
E	Young's modulus [N m^{-2}]
rH	relative humidity of air
T_a	temperature
t	time
$\mathbf{u}$	displacement
X	water content of sample
x, $\hat{x}$	initial and actual coordinates of a point
Y	absolute air moisture.

Subscripts

a	air
eq	equilibrium
in	initial
s	adiabatic saturation
vp	viscoplastic.

Superscripts

$\overline{}$	average over distance
$\tilde{}$	tensor.

Greek symbols

α^*	equivalent mass exchange coefficient
γ	fluidity parameter
ε	strain
ν	Poisson's ratio
σ	stress [N m^{-2}]
φ	angle of internal friction.

initial water content, we have fixed the initial state of the sample near that of the tile before drying: 20% water content (d.b.), volumic mass 2×10^3 kg m^{-3}.

2.1. *Drying kinetics*

Clay samples are subjected to a controlled drying air, with temperature, moisture and velocity given. The samples are discs of 1 cm thickness and 8 cm diameter whose lateral side is protected by a plastic film; in this way, the evaporation is effected through the two faces (Fig. 1). The inlet and outlet air velocities in the sample container are horizontal to avoid air thrust on the electronic scale. The mass is consistently recorded on a P.C. computer which treats the data and delivers conventional kinetics $\dot{\bar{X}} = f(X)$ (Fig. 2). The dry mass is obtained after a stay of 24 h in an oven at 120°C.

In order to avoid a transient phase of temperature increase, the initial temperature of the sample is close to that of the air wet bulb. Figure 2 shows two particular features of drying for this material: one does not observe an initial period of constant rate and the curve is roughly straight with a slight change in the slope around 11% water content. We notice that this value is very near the shrinkage limit (Fig. 12). The absence of a constant rate period is probably brought about by reduced initial water content and mineralogical constitution of the clay. However, with another species of clay and an initial water content of 35%, Kameï [6] obtains a constant rate period.

2.2. *Sorption curves*

As the material is hygroscopic, the equilibrium curves provide data used to express undimensional kinetics. These were determined by weighing small samples resting for 10 days in air-controlled salty solutions. These curves are strongly dependent on mineral composition (Fig. 3). The temperature slightly modifies the shape of the curve and in order to adjust the results, Chung and Pfost's [7] expression is adequate:

$$X_{eq} = -1.95 \ln [-3.96 \times 10^{-4} T_a \ln rH] \quad (1)$$

where rH is the relative humidity of air.

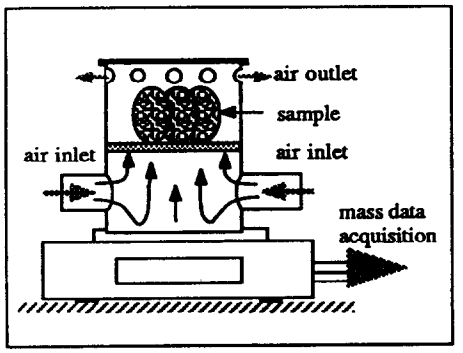

FIG. 1. Sketch of drying apparatus.

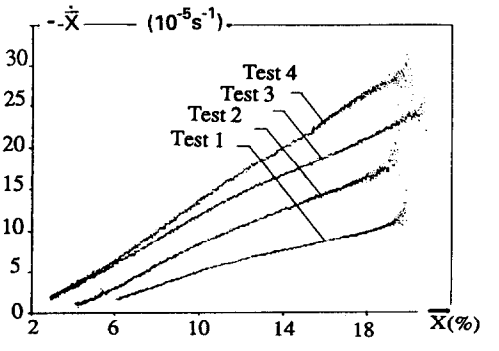

FIG. 2. Drying rate distribution with water content.

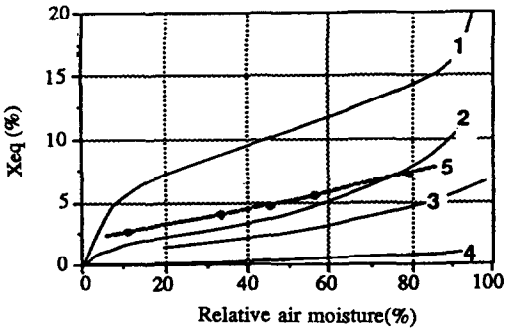

FIG. 3. Sorption curves of some special clays: 1, montmorillonite (Limousin, France); 2, fine illite (region of Paris); 3, kaolinite + illite (Charente, France); 4, pure kaolin (Arvor); 5, clay provided by the French manufacturer (TbF).

2.3. *Drying model*

A linear kinetic curve is convenient for giving an interpretation with a diffusive model. The diffusion equation:

$$\frac{\partial X}{\partial t} = D\nabla^2 X \qquad (2)$$

where D is an equivalent diffusion coefficient, allows for some analytical solutions which depend on boundary conditions.

We consider a one-dimensional drying perpendicular to a plate of thickness $2e$, from an initial uniform water content X_{in}, i.e. $X = X(x, t)$. Two kinds of boundary conditions are generally chosen:

(a) An instantaneous equilibrium of water content at the free surface $X(e, t) = X(-e, t) = X_{eq}$, where $X_{eq} = X_{eq}(T_a, Y)$. The latter condition would be exact if the characteristics T_a, Y were those of the air in contact with the plate surface and not those of the outer part of the boundary layer. At the beginning of drying $X(e, t)$ decreases with a certain delay from X_{in} to X_{eq}, as we can see from the results of Kameï (Fig. 4), and consequently the boundary condition is only adequate at the end of drying (Fig. 5). Furthermore, only parameter D would be adjusted with air temperature and moisture.

(b) An equivalent boundary layer condition at the free surfaces such as

$$-D\frac{\partial X}{\partial x}(\pm e, t) = \alpha^*(X(\pm e, t) - X_{eq}). \qquad (3)$$

The physical justification of this condition is to presuppose a surface drying potential from hygroscopic equilibrium. One can think that this condition is appropriate at the beginning of the drying, with an adjustment of the coefficient α^*. For example, the experiments of Kameï (Fig. 4) show that the surface water content is large with respect to X_{eq} until 7 h, thus allowing a significant definition of α^*. After this time the water content rapidly reaches X_{eq}. As we require great accuracy at the beginning of the drying,

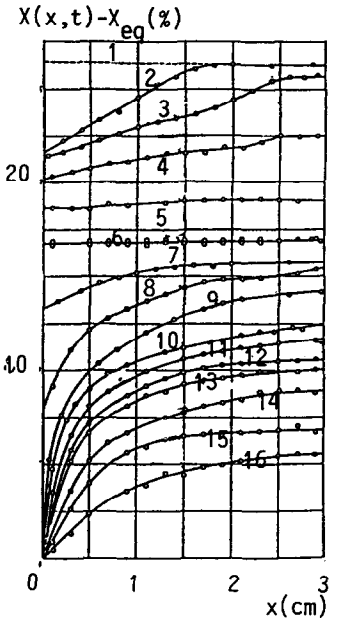

FIG. 4. Water content moisture profiles measured by Kameï [6]. Sample of Minokaolin.

Curve	1	2	3	4	5	6	7	8
ying time (h)	<1	1	2	3	4	5	6	7
Curve	9	10	11	12	13	14	15	16
Drying time (h)	8	10	13	15	17	20	30	40

$T_a = 40°C$; $V = 4\ m\ s^{-1}$; $rH = 0.30$.

1115

when the deformation is larger, we select the boundary condition (b). Moreover, with two adjustable parameters, the agreement with the drying curve would be excellent. The analytical solution (see p. 60 of ref.

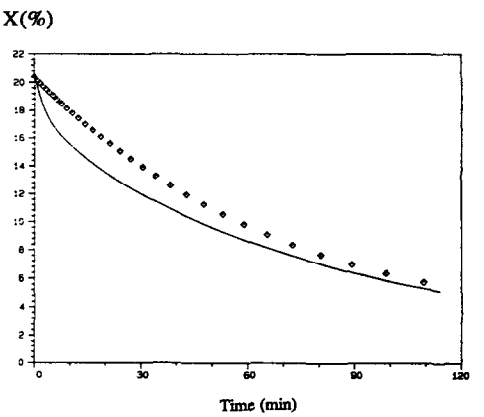

FIG. 5. Diffusive model with only a constant diffusive coefficient as parameter. Drying rate comparison: (◇) experiment; (——) simulation.

[8]) leads to:

$$\frac{X(x,t)-X_{eq}}{X_{in}-X_{eq}} = 2L\sum_{n=1}^{\infty}\frac{1}{(\beta_n^2+L^2+L)\cos\beta_n} \times\cos\left(\frac{\beta_n}{e}x\right)\exp\left[-\frac{\beta_n^2}{e^2}Dt\right] \quad (4)$$

or after an integration:

$$\frac{\bar{X}-X_{eq}}{X_{in}-X_{eq}} = 2L^2\sum_{n=1}^{\infty}\frac{1}{(\beta_n^2+L^2+L)\beta_n^2}\exp\left[-\frac{\beta_n^2}{e^2}Dt\right] \quad (5)$$

where β_n are positive roots of the transcendent equation

$$\beta_n\tan(\beta_n) = L \quad \text{with } L=\frac{e\alpha^*}{D}.$$

The water content profiles are programmed on a computer with a series of 10 terms. For adjustment of the two parameters D and α^*, we can consider that the first term of the series is sufficient after a fixed time. For the samples chosen, after 20 min of drying, this term represents more than 98% of the sum. With this first term only, equation (5) becomes:

$$\ln\bar{X}_+ = -\frac{\beta_1^2 D}{4e^2}t+\ln\left[\frac{2L^2}{(\beta_1^2+L^2+L)\beta_1^2}\right] \quad (6)$$

where

$$\bar{X}_+ = \frac{\bar{X}-X_{eq}}{X_{in}-X_{eq}}.$$

Constant values of D and α^* are not adequate to give a perfect coincidence between the calculated and experimental drying rate curves. It is convenient to define an air characteristic varying with the temperature T_a and the drying potential $Y_S - Y_a$ [9]. Good accuracy is obtained when the diffusion coefficient D is a function of T_a (Fig. 6(a)) and the equivalent exchange coefficient α^* is a function of $Y_S - Y_a$ (Fig. 6(b)). The range of D values is very close to the results of Evans and Keey [10] with Hyde Clay. The coefficients D and α^* being so determined it is possible to obtain a computer drawing of the moisture profiles (Fig. 7(a)) and drying rate (Fig. 7(b)).

The roughly parabolic profiles are similar to those of Kameï (Fig. 4) from 5 h on. Before the limit of ~5 h the Kameï results are doubtful. There is no reason for the evolution of the profile starting from a uniform state (1) to reach another quasi-uniform state (6), after some distorted profiles. This is probably due to variations of experimental conditions. As the water content is obtained with cutting, each curve is relative to a different sample, so conditions may be different for the samples denoted 2, 3 and 4.

One can also compare Kameï profiles with other experimental results (see for example ref. [11]). With the external air characteristic constant the initial uniform moisture content never again becomes uniform during drying. The comparison is also interesting at the end of drying. It seems that a drying front does not appear at the end of drying in the thickness of the plate. This would mean that the material cannot be considered as a capillary-porous medium but rather as a diffusive medium.

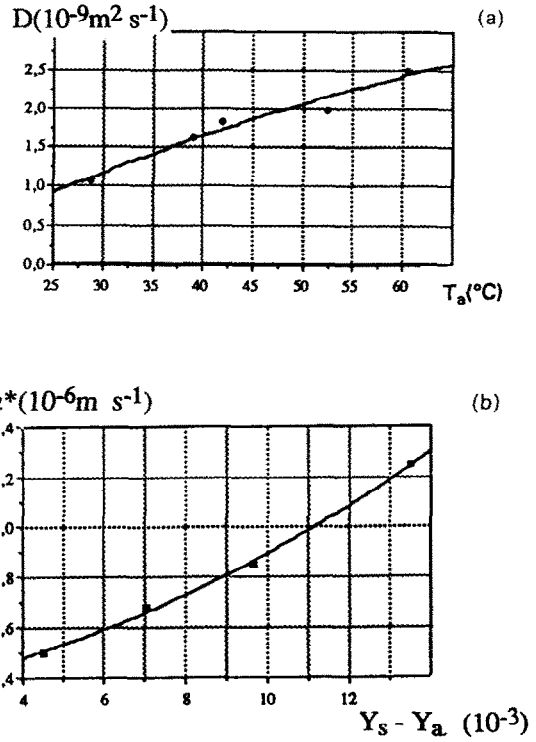

FIG. 6. (a) Diffusion coefficient dependence on temperature. (b) Dependence of equivalent exchange coefficient α^* on drying potential.

3. CONSTITUTIVE MODEL OF THE CLAY PLATE

During drying the kneading paste changes into a hard material with a rock-like consistency. The behaviour of the clay pieces with shrinkage-induced stresses will not be identical at the beginning or the end of drying. The rheological parameters will act as functions of the water content.

3.1. *Properties of the material*

Experiments carried out on this material show that deformations are in part irreversible. The elastic model is not adequate. The plastic and viscous properties can be shown by specific experiments with a triaxial apparatus for compression tests of soil samples. The rate of loading platforms is fixed by the operator. The cylindrical sample is submitted to a uniform pressure on its lateral surface and a normal stress on the circular base sections.

The curves obtained from the stress vs strain of a clay sample show (Fig. 8) that the elastic domain is

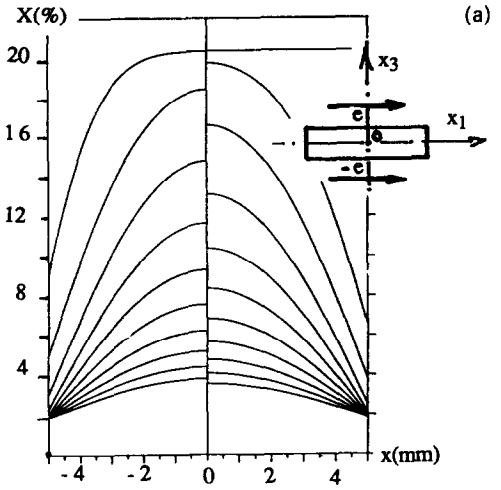

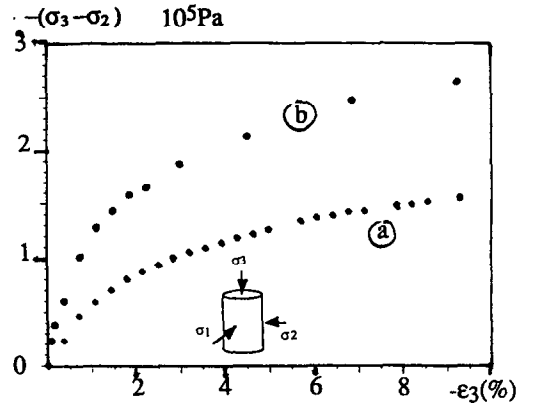

FIG. 9. Influence of the rate of loading on the deformation. $X = 20\%$; $\sigma_1 = \sigma_2 = -10^5$ Pa; (a) $\dot{\varepsilon}_3 = -1.16 \times 10^{-5}\ s^{-1}$; (b) $\dot{\varepsilon}_3 = -39.4 \times 10^{-5}\ s^{-1}$.

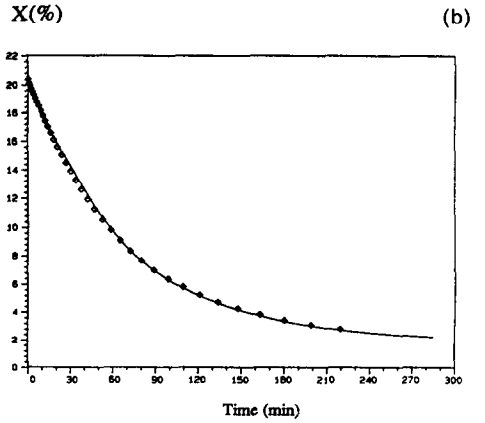

FIG. 7. (a) Moisture profile evolution during drying. Period between two curves: $\Delta t = 2$ min; $T_a = 60°C$; $V = 0.38\ m\ s^{-1}$; $rH = 0.07$. The drying is symmetrical with respect to the x_1 axis. (b) Diffusive model with two adjustable parameters $D(T_a)$ and $\alpha^*(Y_S - Y_a)$. Drying rate: (◇) experiment; (——) simulation.

very limited. The length of the plastic range increases with water content. The viscous effects are obvious when the rate of loading varies (Fig. 9). The stress is a function of the rate of straining. This effect is also noticeable on creep tests (Fig. 10). For a fixed stress state, delayed strains appear.

3.2. *Equations of the model*

This model is supposed to describe phenomena of elasticity, plasticity, and creep in the material. We consider that the viscosity does not appear in the elastic domain. The constitutive law establishes a correspondence from the space of stress to the space of strain rate and vice versa. When the representative point in the stress space leaves the elastic domain, its position is a function of the rate of strain. Thus we divide the total strain into two parts:

$$\varepsilon_t = \varepsilon_e + \varepsilon_{vp}$$

and the viscoplastic strain rate is expressed as [12, 13]

$$\dot{\varepsilon}_{vp} = \gamma\langle\phi(F)\rangle\frac{\partial F}{\partial \sigma} \tag{7}$$

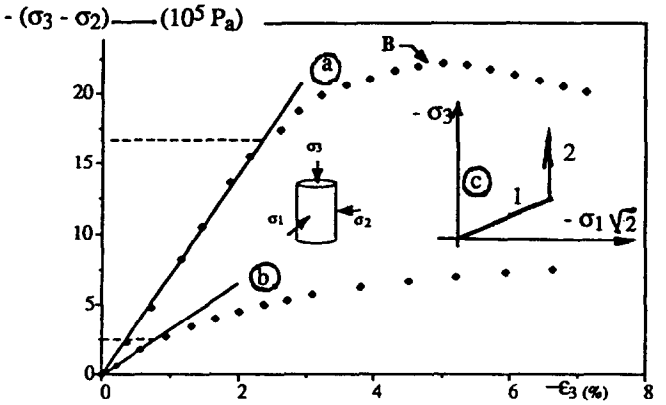

FIG. 8. Deformation of a clay sample submitted to compression stress. $\sigma_1 = \sigma_2 = -3 \times 10^5$ Pa; $\dot{\varepsilon}_3 = -1.16 \times 10^{-5}\ s^{-1}$; (a) $X = 8.8\%$; (b) $X = 14.7\%$. Point B, breaking of the sample.

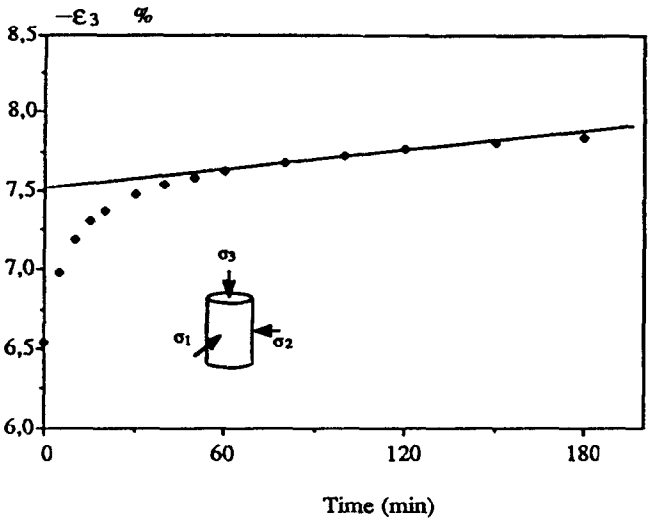

FIG. 10. Creep test on a cylindrical sample. $X = 20.4\%$; $\sigma_1 = \sigma_2 = -3 \times 10^5$ Pa; $\sigma_3 = -5.1 \times 10^5$ Pa.

where F is a yield function; $F < 0$ denotes the purely elastic region. To ensure no viscoplastic flow below the yield limit the function $\langle\ \rangle$ is defined as

$$\langle \phi(F) \rangle = 0 \qquad \text{if } F \leqslant 0$$

$$\langle \phi(F) \rangle = \phi(F) \quad \text{if } F > 0$$

and the function $\phi(F)$ is chosen as the power function (this is sufficiently general to fit the experimental data)

$$\phi(F) = \left(\frac{F}{F_0}\right)^n \tag{8}$$

where F_0 denotes any convenient reference value of F.

In equation (7) γ is a fluidity parameter (inverse of plastic viscosity) which depends on water content, $\partial F/\partial \sigma$ giving the plastic strain rate direction characterizes the 'associated' plastic behaviour. We chose the Mohr–Coulomb criterion, useful in soil mechanics, in order to express the yield limit

$$F = \tfrac{1}{2}(\sigma_1 - \sigma_3) + \tfrac{1}{2}(\sigma_1 + \sigma_3)\sin\varphi - C\cos\varphi \tag{9}$$

where σ_1, σ_3 are the principal stresses (minimum and maximum), C is cohesion and φ is the angle of internal friction. The parameters C and φ are functions of the moisture content and will be determined from specific experiments.

3.3. *Experimental determination of mechanical parameters*

There are six parameters which are introduced in the elastic/viscoplastic model: n, γ, C, φ and two classical elasticity moduli, the Young modulus E and the Poisson ratio v. All these parameters are functions of the moisture content of the sample, and many experiments are necessary to determine their variation.

The conventional triaxial tests using cylindrical samples allow one to determine these parameters. The two elasticity constants are deduced from the curves in the elastic domain (Fig. 8). The relation between the stress σ_3 and the strain ε_3

$$E\varepsilon_3 = +\sigma_3 - v(\sigma_1 + \sigma_2); \quad \sigma_1 = \sigma_2 \tag{10}$$

shows that E is the slope of the curve as the axial compression increases while $\sigma_1 = \sigma_2 = \text{const.}$ (branch 2, Fig. 8).

The dependence of E on moisture content is given in Fig. 11 and shows, obviously, a decrease when the moisture increases. The Poisson ratio is estimated from the work of Scheuch [14] on clays of the Serre-Ponçon dam (Fig. 11).

The parameters of the Mohr–Coulomb yield criterion result from the limit Mohr circles. The dependence of C and φ is given in Fig. 11. These curves demonstrate the increase of plasticity with moisture content.

The viscoplasticity parameters are deduced from the creep curves by the following method. The constitutive law (7) can be expressed as follows in relation to the triaxial test (see for example ref. [15]):

$$\dot{\varepsilon}_{vp11} = \gamma\left(\frac{F}{F_0}\right)^n \frac{1}{4}\left[\left(1 + \frac{\sin\varphi}{3}\right)\frac{\sigma_1}{|\sigma_1 - \sigma_3|} + \sin\varphi - 1\right]$$

$$\dot{\varepsilon}_{vp22} = \dot{\varepsilon}_{vp11}$$

$$\dot{\varepsilon}_{vp33} = \gamma\left(\frac{F}{F_0}\right)^n \left(\tfrac{1}{6}\sin\varphi - \tfrac{1}{2}\right)$$

$$\dot{\varepsilon}_{vp12} = \dot{\varepsilon}_{vp13} = \dot{\varepsilon}_{vp23} = 0 \tag{11}$$

where $F_0 = C\cos\varphi$ and F is given by equation (9). γ and n are obtained from several load paths by measuring $\varepsilon_{vp33}(t)$ for samples of given humidity. The dependence on moisture content is indicated in Fig. 11 and it is evident that fluidity is an accurate term for γ.

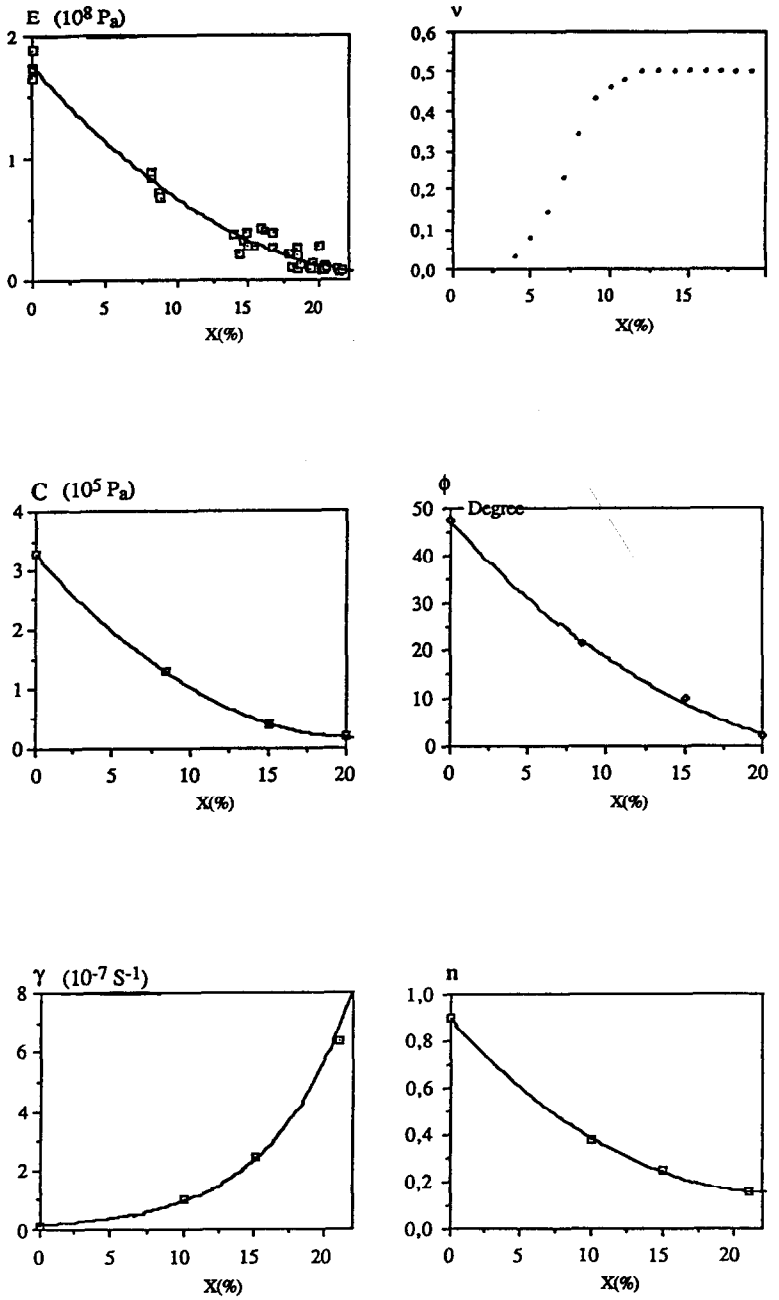

FIG. 11. Dependence of the rheologic model parameters upon moisture content: Young's modulus, Poisson ratio, cohesion parameter, angle of internal friction, viscoplasticity parameters γ and n.

4. NUMERICAL STUDY OF THE DEFORMATION OF A CLAY PLATE DURING DRYING

We have to associate the rheological and drying models in order to describe the deformation of a model clay plate. The boundary conditions are chosen to amplify the deformation. Consider the horizontal plate; its upper face is submitted to the drying air whose parameters are the temperature T_a and one of the three data: relative humidity rH, absolute humidity Y_a or drying potential $Y_S - Y_a$. The lower and lateral faces are isolated (impervious and adiabatic). The gravity effect and initial stress are supposed negligible with respect to stresses induced by shrinkage.

4.1. *The inverse method*

As the general rate boundary-value problem of drying for the elastic/viscoplastic plate is complex to carry out, we choose the inverse simplified method which

consists of postulating a general form of displacement field and then identifying the unknown coefficients. If a solution exists, we suppose its uniqueness.

With the guideline of a commonly observed form of plate, we presuppose a displacement field as follows:

$$\mathbf{u} = \begin{bmatrix} u_1 = b(x_3)x_1 \\ u_2 = b(x_3)x_2 \\ u_3 = a(x_3)+c(x_3)(x_1^2+x_2^2) \end{bmatrix} \quad (12)$$

which means that the upper surface has a revolution paraboloid. The coefficients a, b and c are to be determined from the equilibrium and constitutive equations.

The boundary conditions on the surface $x_3 = e$ and $x_3 = 0$ (the latter represents the mean surface for the diffusion problem of Section 2) are:

$$\sigma_{33} = 0; \quad \sigma_{23} = 0; \quad \sigma_{13} = 0.$$

4.2. *Expression of stress and strain tensor*

Having assumed the kinematics of the plate with an adapted coordinate system, the total strain tensor is expressed by its components, as follows:

$$\varepsilon_{ij} = \frac{1}{2}\left(\frac{\partial u_i}{\partial x_j} + \frac{\partial u_j}{\partial x_i}\right)$$

$$\varepsilon_{11} = \varepsilon_{22} = b$$

$$\varepsilon_{33} = a' + c'r^2; \quad r^2 = x_1^2 + x_2^2$$

$$\varepsilon_{13} = \tfrac{1}{2}(2c+b')x_1$$

$$\varepsilon_{23} = \tfrac{1}{2}(2c+b')x_2$$

$$\varepsilon_{12} = 0. \quad (13)$$

We can state that the total strain induced by shrinkage is the sum of shrinkage, elastic and viscoplastic strains:

$$\boldsymbol{\varepsilon}_t = \boldsymbol{\varepsilon}_h + \boldsymbol{\varepsilon}_e + \boldsymbol{\varepsilon}_{vp}. \quad (14)$$

The shrinkage strains induced by the drying in the isotropic medium are represented by normal components (as the thermal ones), i.e.

$$\boldsymbol{\varepsilon}_h = \begin{bmatrix} \varepsilon_h & 0 & 0 \\ 0 & \varepsilon_h & 0 \\ 0 & 0 & \varepsilon_h \end{bmatrix}$$

where ε_h is the strain deduced from the shrinkage curve. In Fig. 12 the shrinkage curve is represented for a standard bar as the ratio of the actual length $\mathbf{I}$ and the dry one $\mathbf{I}_d$ vs water content. In the case of a sample of initial content X_{in}, the curve gives $\mathbf{I}_{in}/\mathbf{I}_d$, and the component ε_h is deduced:

$$\varepsilon_h = 1 - \frac{\mathbf{I}}{\mathbf{I}_d} \Big/ \frac{\mathbf{I}_{in}}{\mathbf{I}_d}.$$

The viscoplastic strain tensor is expressed as

$$\boldsymbol{\varepsilon}_{vp} = \begin{bmatrix} \varepsilon_{vp11} & 0 & \varepsilon_{vp13} \\ 0 & \varepsilon_{vp22} & \varepsilon_{vp23} \\ \varepsilon_{vp13} & \varepsilon_{vp23} & \varepsilon_{vp33} \end{bmatrix}.$$

As for the total strain tensor $\varepsilon_{11} = \varepsilon_{22}$, we keep here $\varepsilon_{vp11} = \varepsilon_{vp22}$.

The stress tensor is generated by elasticity, i.e. $\boldsymbol{\sigma} = C:\ \boldsymbol{\varepsilon}_e = C:\ (\boldsymbol{\varepsilon}_t - \boldsymbol{\varepsilon}_h - \boldsymbol{\varepsilon}_{vp})$, where C is the elastic stiffness matrix. For an isotropic medium considered here, we have $\sigma_{ij} = \lambda\delta_{ij}\theta_e + 2\mu\varepsilon_{eij}$ where δ_{ij} is the Kronecker symbol and

$$\lambda = \frac{Ev}{(1+v)(1-2v)}; \quad \mu = \frac{E}{2(1+v)}$$

$$\theta_e = \varepsilon_{eii}. \quad (15)$$

λ and μ are x_3 functions through $E(X)$, $v(X)$ (Fig. 11) and $X(x_3)$.

Taking into account equations (13) and (14) the elastic stress tensor becomes:

$$\sigma_{11} = \lambda(a' + c'r^2) + 2(\lambda+\mu)(b - \varepsilon_{vp11}) - (3\lambda+2\mu)\varepsilon_h - \lambda\varepsilon_{vp33}$$

$$\sigma_{22} = \sigma_1$$

$$\sigma_{33} = (\lambda+\mu)(a' + c'r^2) + 2\lambda b - (3\lambda+2\mu)\varepsilon_h - 2\lambda\varepsilon_{vp11} - (\lambda+2\mu)\varepsilon_{vp33}$$

$$\sigma_{12} = 0$$

$$\sigma_{13} = \mu(2c+b')x_1 - 2\mu\varepsilon_{vp13}$$

$$\sigma_{23} = \mu(2c+b')x_2 - 2\mu\varepsilon_{vp23}. \quad (16)$$

The associated static equilibrium equations are:

$$\frac{\partial \sigma_{ij}}{\partial x_j} + S_i = 0 \quad (17)$$

where $S(S_1, S_2, S_3)$ is the external body force density per unit volume. As we consider body forces, e.g. the gravity forces, to be negligible with respect to the drying effects, the vector S is taken as null.

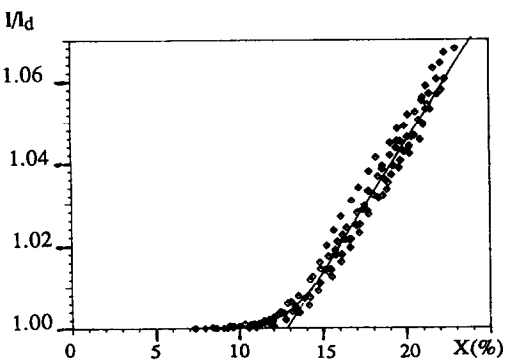

FIG. 12. Shrinkage curve of a cylindrical sample. The shrinkage limit is taken as 12.8%.

4.3. *Simplified solution*

At this point, we consider that the elastic stress tensor is a function of x_3 only. This hypothesis, verified for a purely elastic material, is in agreement with the drying model where moisture varies only in the direction perpendicular to the plate. Then, equations (16) and (17) can be simplified: $c' = 0$ means that c is a constant and

$$\frac{\partial \sigma_{13}}{\partial x_3} = \frac{\partial \sigma_{23}}{\partial x_3} = \frac{\partial \sigma_{33}}{\partial x_3} = 0;$$

in accord with the boundary conditions $\sigma_{13} = \sigma_{23} = \sigma_{33} = 0$.

The expression of σ_{13}, σ_{23} gives

$$\varepsilon_{vp13} = \varepsilon_{vp23} = 0$$
$$2c + b' = 0.$$

The integration of this last equation gives

$$b = b_0 - 2cx_3. \tag{18}$$

The expression of the coefficient a' is deduced from σ_{33}, and the stress tensor becomes

$$\sigma_{11} = \alpha(b - \varepsilon_h - \varepsilon_{vp11}); \quad \alpha = 2\mu\frac{3\lambda+2\mu}{\lambda+2\mu}$$
$$\sigma_{22} = \sigma_1$$
$$\sigma_{33} = 0$$
$$\sigma_{12} = \sigma_{13} = \sigma_{23} = 0. \tag{19}$$

We use further the global equilibrium equations for a section:

$$\int_0^e \sigma_{11}\,dx_3 = 0; \quad \int_0^e x_3\sigma_{11}\,dx_3 = 0.$$

The reaction of the support is negligible, as is the gravity. With equations (18) and (19) these equations give:

$$b_0\int_0^e \alpha\,dx_3 - 2c\int_0^e \alpha x_3\,dx_3 = \int_0^e \alpha(\varepsilon_h + \varepsilon_{vp11})\,dx_3$$
$$b_0\int_0^e \alpha x_3\,dx_3 - 2c\int_0^e \alpha x_3^2\,dx_3 = \int_0^e \alpha(\varepsilon_h + \varepsilon_{vp11})x_3\,dx_3. \tag{20}$$

These last equations determine the values of b_0 and c for each x_3 position. The coefficient α is a function of x_3 through the local water content (equations (15) and (19)). The component ε_h is directly expressed by X; the component ε_{vp11} is obtained by an integration of $\dot{\varepsilon}_{vp}$ (equations (7) and (11)).

The global deformation results from the knowledge of b_0 and c. The equations of the plate are:

$$\hat{x}_1 = x_1 + u_1 = x_1 + (b_0 - 2cx_3)x_1$$
$$\hat{x}_2 = x_2 + u_2 = x_2 + (b_0 - 2cx_3)x_2$$
$$\hat{x}_3 = x_3 + u_3 = x_3 + a(x_3) + c(x_1^2 + x_2^2)$$

and gives for the surface $x_3 = 0$, the paraboloid:

$$\hat{x}_3 = \frac{c}{(1+b_0)^2}(\hat{x}_1^2 + \hat{x}_2^2). \tag{21}$$

The radius of curvature is $R = -(1+b_0)^2/2c$.

5. THE NUMERICAL RESOLUTION OF THE DRYING AND DEFORMATION PLATE

The boundary conditions are those described above: one face submitted to drying air and the other face impervious. The computer programme gives the water content, stress and deformation profiles at each step in time.

The procedure adopted is as follows:

- Loop on time
  - $t = t + \Delta t$
  - loop on space
    - $x = x + \Delta x$
    - $X(x, t)$ (equation (4))
    - $E, \nu, C, \varphi, \gamma, n, \varepsilon_h$ (Fig. 11)
    - F (equation (9), $\sigma_3 = 0$)
    - $\dot{\varepsilon}_{vp11}$ (equation (11), $\sigma_3 = 0$)
    - $\varepsilon_{vp11} = \dot{\varepsilon}_{vp11}\Delta t$
  - b_0, c (equation (20))
  - $\sigma_{11}(x, t)$ (equation (19))
  - R (equation (21)).

The evolution of the drying and stress fields is indicated in Fig. 13.

At the beginning of drying, the shrinkage provokes traction stress near the surface and compression stress in the middle of the plate. We then notice an inversion of the stress sign. Near the drying end, the two faces of the plate are submitted to a compression, and the middle to a traction.

Figure 14 focuses on the stress at the surfaces $x_3 = 0$, $x_3 = e$ and in the mid-thickness in the function of time. With this kind of drying, the upper face stress attains maximum values at the beginning of drying. The first moments of drying are critical for crack initiation.

6. EXPERIMENTAL STUDY OF PLATE DEFORMATION DURING DRYING

A clay plate of $215 \times 215 \times 10$ mm made of the material used in previous experiments was set down on the floor of a wind tunnel where the air characteristics are controlled. A plastic film assured the impermeability on the faces which must not dry. A foam bed assured a continuous contact on the lower face. At the beginning, the plate curves into a spherical shape and its extreme edges lift up. The curvature radius reaches a maximum, then decreases and changes its sign. The concavity is now directed towards the wall support. The numerical results conform with the experimental ones (Fig. 15), but we notice some differences at the beginning of drying. We

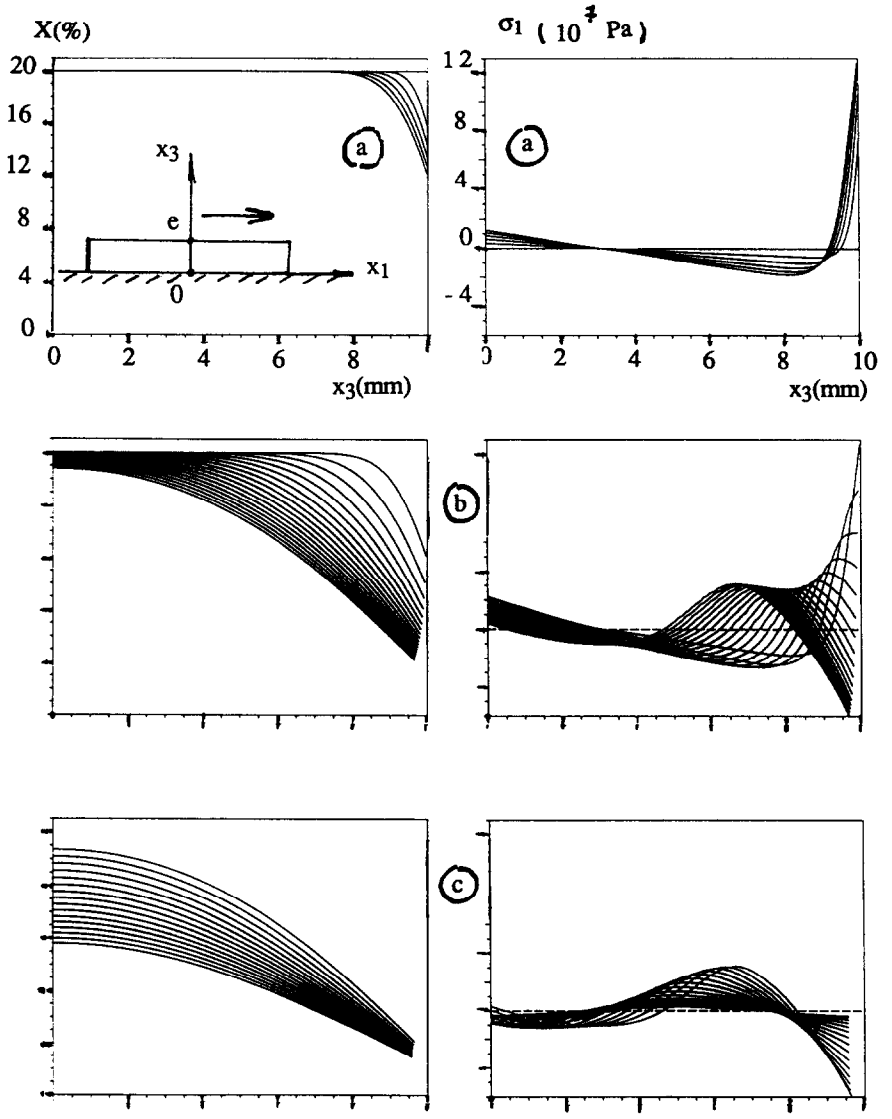

FIG. 13. Evolution of the water content and the stress profiles during drying. (a) $0 \leqslant t \leqslant 5$ mm; $\Delta t = 1$ min. (b) $5 \leqslant t \leqslant 113$ mm; $\Delta t = 6$ min. (c) $113 \leqslant t \leqslant 338$ mm; $\Delta t = 15$ min.

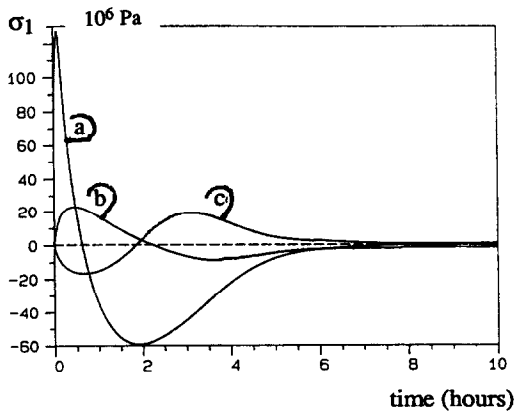

FIG. 14. Evolution of the stress σ_1, on the faces and the middle of the plate. (a) The stress on the drying face. (b) The stress on the impervious face. (c) The stress on the median plane.

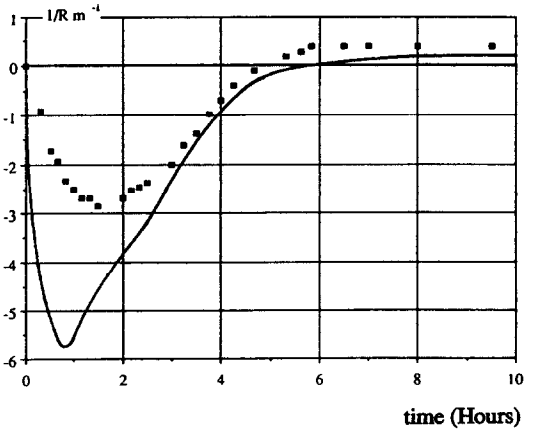

FIG. 15. Comparison of the experimental and numerical results. Evolution of the curvature.

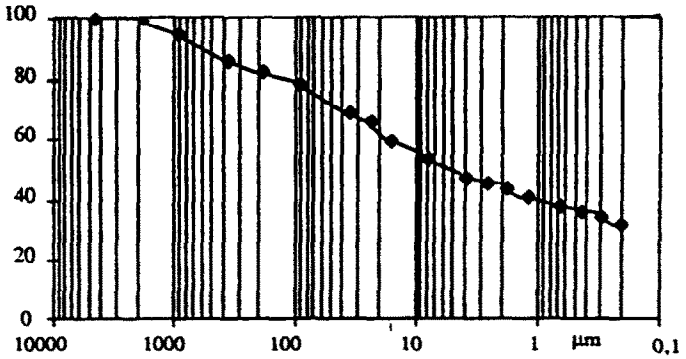

FIG. 16. Cumulative mass percentage vs particle diameter.

attempt an explanation of the distortion through the drying or deformation model. The drying model is correctly adjusted on the experimental rates, but we note that the characteristics of the boundary layers close to the samples are different for the two kinds of experiments (drying rate and deformation). The mean flow rate V is perhaps not a sufficient parameter to express (with T_a, Y_a) the air characteristics. The viscoplastic model involves two parameters, γ and n, determined from mean curves of creeping tests (Fig. 10) and does not account for the initial phase. 1115

7. CONCLUSION

The associated problem of drying and deformation has found a satisfactory simplified solution here for the case of a plate of simple geometry, made of a complex material. Indeed, if the drying model needs only two parameters (D, α^*), the deformation model is expressed with seven parameters (E, ν, C, φ, λ, n, ε_h) which are functions of the water content. Of course, an elastic model is not adequate to deliver a permanent deformation after drying. A viscoplastic model is more realistic for such materials. It is pointed out that all the parameters relevant to the rheology at stake are determined from specific experiments (and are not identified on a global scale).

It seems that a better agreement between simulation and experiment would be obtained with more refined models. An adaptation of the most sensible parameters as α^* to account for features of boundary layer and γ or n for viscous properties may be recommended. So, the next step for industrial applications will be to treat particular geometries of the manufacturing pieces.

Acknowledgement—The French manufacturer 'Tuiles et Briques Françaises' kindly provided the clay paste used for the experimental procedure.

REFERENCES

1. S. Whitaker, Heat and mass transfer in granular porous media. In *Advances in Drying* (Edited by S. Mujumbar), Vol. 1, p. 23. Hemisphere, New York (1980).
2. S. Ben Nasrallah and P. Perre, Detailed study of a model of heat and mass transfer during convective drying of porous media, *Int. J. Heat Mass Transfer* **31**, 957–967 (1988).
3. G. C. Sih, J. G. Michopoulos and S. C. Chou, *Hygrothermoelasticity*. Martinus Nijhoff, The Netherlands (1986).
4. G. Y. Baladi and B. Rohani, *Development of an Elastic–Viscoplastic Constitutive Relationship for Earth Materials in Mechanics of Engineering Materials* (Edited by C. S. Desai and R. H. Gallagher), Chap. 2, p. 23. Wiley, New York (1984).
5. R. W. Lewis, K. Morgan and H. R. Thomas, The non linear modeling of drying induced stresses in porous bodies. In *Advances in Drying* (Edited by A. S. Mujumbar), Vol. 2, Chap. 7, p. 233. Hemisphere, New York (1983).
6. S. Kameï, quoted by O. Krischer and K. Kröll, *Die wissenschaftlichen grundlagen der Trocknungstechnik*, Translation of CETIAT, p. 382. Springer, Berlin (1956).
7. D. S. Chung and H. B. Pfost, quoted by M. Fortes and M. R. Okos, *Advances in Drying* (Edited by A. S. Mujumbar), Vol. 1, Chap. 5, p. 122. Hemisphere, New York (1980).
8. S. Crank, *The Mathematics of Diffusion*. Clarendon Press, Oxford (1975).
9. R. B. Keey, *Drying Principles and Practice*. Pergamon Press, Oxford (1972).
10. A. A. Evans and R. B. Keey, The moisture diffusion coefficient of a shrinking clay on drying, *Chem. Engng J.* 127–134 (1975).
11. J. Van Brakel, Mass transfer in convective drying. In *Advances in Drying* (Edited by A. S. Mujumbar), Vol. 1, p. 217. Hemisphere, New York (1980).
12. L. E. Malvern, *J. Appl. Mech.* **18**, 203 (1951).
13. P. Perzyna, Fundamental problems in viscoplasticity, *Adv. Appl. Mech.* **9**, 243 (1966).
14. G. Scheuch, Contribution à l'étude des argiles non saturés, Thèse à la Faculté des Sciences de Grenoble, France (1959).
15. D. R. Owen and E. Hinton, *Finite Elements in Plasticity, Theory and Practice*. Pineridge Press, Swansea (1980).

DEFORMATIONS D'UNE PLAQUE D'ARGILE INDUITES PAR LE SECHAGE

Résumé—L'objet de cet article est l'étude du séchage et de la déformation d'une plaque d'argile soumise sur une de ses faces à l'action d'un courant d'air. Le modèle de séchage adopté est un modèle diffusif dont les coefficients sont ajustés sur les cinétiques de séchage. Le modèle contraintes/déformations est élastique–viscoplastique dont le critère de plasticité est celui de Mohr–Coulomb. Les six coefficients de ce modèle sont obtenus à partir d'expériences spécifiques de retrait, compression triaxiale, fluage. Ces coefficients sont des fonctions de la teneur en eau locale, ce qui établit la liaison entre les deux modèles. Les résultats du calcul sont en bon accord avec la déformation globale mesurée de la plaque.

TROCKNUNGSBEDINGTE DEFORMATION EINER LEHMPLATTE

Zusammenfassung—Inhalt der Untersuchung sind die durch den Trocknungsprozeß verursachten Deformationen einer Lehmplatte, welche einseitig durch Luft getrocknet wird. Das Rechenmodell berücksichtigt den Diffusionsvorgang, wobei die Stoffeigemschaften auf die Trocknungskinetik abgestimmt sind. Das Spannungs-/Dehnungs-Verhalten des Materials ist elastisch/viskoplastisch mit einem Ertragskriterium nach Mohr–Coulomb. Die sechs für das Modell benötigten Stoffeigenschaften werden durch verschiedene Einzelversuche ermittelt: Schrumpfung, dreiachsige Kompression einer zylindrischen Probe unter konstanter Last und Kriechversuch. Einige der Eigenschaften sind abhängig von der Feuchtigkeit des Materials und stellen so eine Verbindung zwischen dem Stofftransport und den mechanischen Eigenschaften her. Die Ergebnisse der durchgeführten Berechnungen stimmen mit den experimentellen Resultaten für die Plattendeformation überein.

ДЕФОРМАЦИЯ ГЛИНЯНОЙ ПЛАСТИНЫ В ПРОЦЕССЕ СУШКИ

Аннотация—Исследуется деформация глиняной пластины, одна сторона которой подвергается сушке воздухом. Модель сушки является диффузионной с коэффициентами, вычисленными по кинетике сушки. Соотношение между напряжением и деформацией является характерным для упругих вязко-пластичных сред и содержит критерий текучести Мора–Кулона. Получены шесть соответствующих коэффициентов для материала при экспериментах по усушке и трехмерному сжатию цилиндрических образцов в условиях постепенного нагружения и ползучести. Некоторые коэффициенты зависят от влажности, т.е. имеется взаимосвязь между массопереносом и механическими полями. Результаты расчетов согласуются с экспериментальными данными по деформации пластины.